Probability of noise- and rate-induced tipping

Paul Ritchie[1,*] and Jan Sieber[1,2,†]

[1]*Centre for Systems, Dynamics and Control, College of Engineering, Mathematics and Physical Sciences, Harrison Building, University of Exeter, Exeter EX4 4QF, United Kingdom*

[2]*EPSRC Centre for Predictive Modelling in Healthcare, University of Exeter, Exeter EX4 4QJ, United Kingdom*

(Received 16 January 2017; revised manuscript received 12 April 2017; published 12 May 2017)

We propose an approximation for the probability of tipping when the speed of parameter change and additive white noise interact to cause tipping. Our approximation is valid for small to moderate drift speeds and helps to estimate the probability of false positives and false negatives in early-warning indicators in the case of rate- and noise-induced tipping. We illustrate our approximation on a prototypical model for rate-induced tipping with additive noise using Monte Carlo simulations. The formula can be extended to close encounters of rate-induced tipping and is otherwise applicable to other forms of tipping. We also provide an asymptotic formula for the critical ramp speed of the parameter in the absence of noise for a general class of systems undergoing rate-induced tipping.

DOI: 10.1103/PhysRevE.95.052209

I. INTRODUCTION

The notion of tipping describes the phenomenon observed in science, where gradual changes to input levels cause a sudden (in practice possibly catastrophic) change in the output. Examples of tipping in science include Arctic sea ice melting [1], degradation of coral reefs [2], dieback of tropical forest and savanna to a treeless state [3], and financial market crashes [4].

Recently, Ashwin *et al.* [5] attempted to classify the underlying mechanisms behind any observed tipping event as an example of either bifurcation-, noise-, or rate-induced tipping. The case of a slow passage through a bifurcation (often a saddle-node), causing a loss of stability and therefore an abrupt transition to an alternative stable state [6], is called *bifurcation-induced tipping*. In contrast, random (rare) jumps between attractors of an underlying deterministic system due to fluctuations is classified as *noise-induced tipping*. *Rate-induced tipping* occurs when a system fails to track the continuously changing quasisteady state [5] because the parameter drift speed exceeds a certain critical rate. For more general definitions and properties of bifurcation- or rate-induced tipping, we refer to Ashwin *et al.* [7].

A research area related to tipping is the study of generic early-warning indicators [8]. Increase of autocorrelation and variance in output time series are two statistical indicators that are based on the phenomenon commonly known as "critical slowing down" as a system parameter approaches a bifurcation value [9]. The idea is that far from a bifurcation, the state of the system behaves like an overdamped particle in a slowly softening potential well [10]. If a small perturbation is made to the particle there will be a fast recovery back to the equilibrium [11]. However, as the bifurcation is approached, the well softens and the recovery from a small perturbation will be slower such that one generically observes an increase in the autocorrelation and variance in output time series [12]. On the other hand, for purely noise-induced transitions no bifurcation point is approached and therefore there is debate into the usefulness of the early-warning signals for this type of tipping [13,14]. Rate-induced tipping does not involve a loss of stability [15] and therefore Ashwin *et al.* [5] commented that there is no reason to suggest the early-warning indicators should be present. However, it has been shown that for a prototypical model for rate-induced tipping the autocorrelation and variance increase before the closest encounter with the critical rate occurs [10].

In the study of palaeoclimate records [16,17], early-warning indicators have been tested on events in the past when tipping has been known to occur. However, testing the early-warning indicators against historical examples is susceptible to statistical mistakes as one selects data conditioned on the system having tipped [18].

A natural progression will be to use the early-warning indicators to try and predict future tipping events. Though, this raises such questions as, if we were to observe an increase in both the autocorrelation and variance of a time series does this mean that the system will tip? Boettiger and Hastings [19] show there is an increased rate of false positives in early-warning indicators for simulated systems that experience transitions purely by chance. Furthermore, Drake [20] suggests that stochastic switching can be anticipated but argues that any statistics to be used as early-warning requires decision theory to balance the strength of evidence against the cost and benefits of early warnings and false positives.

This paper provides a generic approximation for the probability of a prototypical model for rate-induced tipping with additive white noise. It is structured as follows: Section II gives a general asymptotic approximation for the critical rate for a class of deterministic systems with rate-induced tipping. Section III derives the approximation for the probability of a noise-induced escape during ramp of a system parameter that does not quite reach the critical rate. In Sec. IV, we illustrate the general approximation result with the prototype model introduced by Ashwin *et al.* [5], which we then systematically study in dependence of its parameter in Sec. V. Finally, in Sec. VI we discuss the limits of our approximations and how further developments can address these.

*pdlr201@exeter.ac.uk
†J.Sieber@exeter.ac.uk

II. RATE-INDUCED TIPPING IN SYSTEMS WITH A RAMPED PARAMETER

A general scenario for the phenomenon of rate-induced tipping was considered by Ashwin *et al.* [5,7]. Assume that a parameter λ corresponds to a shift of the coordinate system:

$$\dot{x} = f(x + b\lambda), \quad x(t) \in \mathbb{R}^n, \quad b \in \mathbb{R}^n, \quad \lambda \in \mathbb{R}, \quad (1)$$

where the vector b is the direction of the shift and λ is the (scalar) amount. For each fixed λ the stability of, for example, equilibria of Eq. (1) is identical. However, when λ is time-dependent, then there can be *critical rates* [21] of change of λ.

A. Linear shift

The simplest example discussed in Ashwin *et al.* [5] is a linear parameter shift, that is, $\lambda = r_{\text{lin}}t$ (with $r_{\text{lin}} > 0$ constant). One of the cases studied in Ashwin *et al.* [5] was assuming that the system in comoving coordinates,

$$\dot{y} = f(y) + r_{\text{lin}}b \quad (\text{where } y = x + br_{\text{lin}}t), \quad (2)$$

has a saddle-node bifurcation at $r_{\text{lin}} = r_0 > 0$, $y = y_0$ with a stable branch $y^{(\text{s})}[r_{\text{lin}}]$ and an unstable branch $y^{(\text{u})}[r_{\text{lin}}]$ of equilibria emerging for $r_{\text{lin}} \in [0, r_0)$. (We will be using square brackets to denote branches of equilibria to avoid confusion with time dependence.) These equilibria for y correspond to stable and unstable invariant lines $x^{(\text{s})}(t) = y^{(\text{s})}[r_{\text{lin}}] - br_{\text{lin}}t$, $x^{(\text{u})}(t) = y^{(\text{u})}[r_{\text{lin}}] - br_{\text{lin}}t$ of the original system Eq. (1) for $r_{\text{lin}} \in [0, r_0)$. For $r_{\text{lin}} < r_0$, all initial conditions $x(0)$ near $y^{(\text{s})}[r_{\text{lin}}]$ follow $x^{(\text{s})}(t)$ for all $t > 0$, while for $r_{\text{lin}} > r_0$ this invariant line no longer exists such that the rate r_0 is critical. This scenario corresponds to a saddle-node bifurcation in the comoving coordinates in Eq. (2) using y. Increasing r_{lin} gradually corresponds to a slow passage through a saddle-node bifurcation.

B. Ramped shift

A more complex scenario is the case where λ is "ramped up," that is, $\lambda \to 0$ for $t \to -\infty$, $\lambda \to \lambda_{\max}$ for $t \to +\infty$, and $\dot{\lambda}(t) > 0$ for all t. A prototype system for this ramping scenario was studied in Refs. [5,10] and is used in Sec. IV for illustration. For the one-dimensional case, Ashwin *et al.* [7] gave topological criteria (and a general definition) for rate-induced tipping with a ramped parameter λ. For the general case, Eq. (1), we assume that the change of the ramp in λ is itself given by a scalar differential equation. Define

$$\begin{aligned} r &= \max\{\dot{\lambda}(t) : t \in \mathbb{R}\} && \text{(maximal ramp speed)} \\ \epsilon &= r/\lambda_{\max} && \text{(sharpness of ramp)} \\ \mu(t) &= \lambda(t)/\lambda_{\max} && (\lambda \text{ normalized to } [0,1]), \end{aligned}$$

then, assuming $\dot{\lambda}$ is bounded and using the new parameters r and ϵ, x and μ are the solution of an autonomous extended system:

$$\dot{x} = f\left(x + b\frac{r}{\epsilon}\mu\right), \quad (3)$$

$$\dot{\mu} = \epsilon\Gamma(\mu), \quad (4)$$

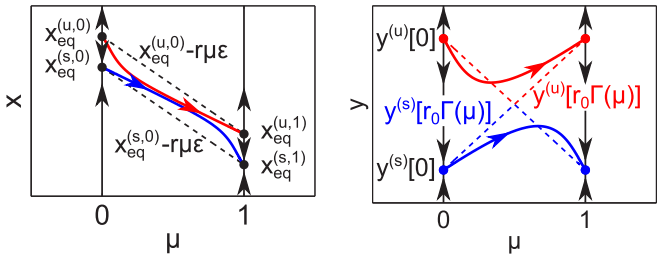

FIG. 1. (a) Phase plane of system Eqs. (3) and (4) for the scenario of tracking, $r < r_c(\epsilon)$. Black dashed lines are the stable (lower) and unstable (upper) branches of equilibria in the limit $\epsilon = 0$. Solid blue and red curves represent connecting orbits between $(x,\mu) = (x_{\text{eq}}^{(\text{s},0)},0)$ and $(x_{\text{eq}}^{(\text{s},1)},1)$ and $(x_{\text{eq}}^{(\text{u},0)},0)$ to $(x_{\text{eq}}^{(\text{u},1)},1)$, respectively. (b) Phase plane of system Eqs. (8) and (9) for $r = r_0$, tracking scenario for $\epsilon > 0$. The blue (lower) dashed line displays the branch of stable equilibria and the red (upper) dashed line is the branch of unstable equilibria in the limit $\epsilon = 0$. Connecting orbits between $(y,\mu) = (y^{(\text{s})}[0],0)$ and $(y^{(\text{s})}[0],1)$, and $(y^{(\text{u})}[0],0)$ and $(y^{(\text{u})}[0],1)$ are given by solid blue and red curves respectively. Parameters: $b = 1$, $\epsilon = 0.21$.

where Γ normalizes $\dot{\lambda}$ to $[0,1]$. Since $\dot{\lambda}$ is always positive, Γ satisfies the following properties

$$\Gamma(0) = \Gamma(1) = 0, \quad \max\{\Gamma(\mu) : \mu \in [0,1]\} = 1, \quad \text{and} \quad \Gamma(\mu) > 0 \text{ for all } \mu \in (0,1). \quad (5)$$

Let us also assume that λ approaches its limits at an exponential rate such that $\Gamma'(0) > 0$, $\Gamma'(1) < 0$, and that Γ is only equal to 1 in a single point $\mu_{\text{crit}} \in (0,1)$ and that $\Gamma''(\mu_{\text{crit}}) < 0$.

If system Eq. (2) has a saddle-node bifurcation at $y = y_0$, $r := r_{\text{lin}} = r_0$, connecting a stable branch $y^{(\text{s})}[r]$ of equilibria of Eq. (2) and a branch $y^{(\text{u})}[r]$ with a single degree of instability for $r \in [0, r_0]$, then we can make the following statement about the existence of a critical rate $r_c(\epsilon)$ for sufficiently small ϵ.

The system Eqs, (3) and (4) have (at least) four equilibria:

(1) $x_{\text{eq}}^{(\text{s},0)} := y^{(\text{s})}[r]|_{r=0}$, $\mu = 0$ with one unstable direction,

(2) $x_{\text{eq}}^{(\text{u},0)} := y^{(\text{u})}[r]|_{r=0}$, $\mu = 0$ with two unstable directions,

(3) $x_{\text{eq}}^{(\text{s},1)} := y^{(\text{s})}[r]|_{r=0} - br/\epsilon$, $\mu = 1$ (stable),

(4) $x_{\text{eq}}^{(\text{u},1)} := y^{(\text{u})}[r]|_{r=0} - br/\epsilon$, $\mu = 1$ with one unstable direction.

For sufficiently small ϵ there are three possible scenarios for system Eqs. (3) and (4) depending on r and a critical rate $r_c(\epsilon)$, illustrated in Fig. 1.

Tracking: $r < r_c(\epsilon)$. There is a connecting orbit from $(x_{\text{eq}}^{(\text{s},0)},0)$ to $(x_{\text{eq}}^{(\text{s},1)},1)$. In this case, solutions $(x(t),\mu(t))$ starting close to $(x_{\text{eq}}^{(\text{s},0)},0)$ stay close to $(x_{\text{eq}}^{(\text{s},0)} - br\mu(t)/\epsilon,\mu(t))$ for all t (the distance goes to 0 as $\epsilon \to 0$); see Fig. 1(a).

Critical: $r = r_c(\epsilon) = r_0 + O(\epsilon)$. There is a saddle-to-saddle connection from $(x_{\text{eq}}^{(\text{s},0)},0)$ to $(x_{\text{eq}}^{(\text{u},1)},1)$ in system Eqs. (3) and (4). The first-order expansion for r_c in ϵ is

$$r_c(\epsilon) = r_0 + \epsilon\sqrt{\frac{-r_0\Gamma''(\mu_{\text{crit}})}{2a_0a_2}} + O(\epsilon^2), \quad (6)$$

where $a_0 = w_0^T b$, $a_2 = \frac{1}{2}w_0^T\partial^2 f(y_0)v_0^2$, and w_0 and v_0 are the left and right null vectors of $\partial f(y_0)$, scaled such

that $w_0^T v_0 = 1$ and $a_0 a_2 > 0$. The coefficients a_0 and a_2 are the expansion coefficients when one inserts $y = y_0 + v_0 z$ and $r_{\text{lin}} = r\Gamma(\mu) - r_0$ into Eq. (2), applies w_0^T, and truncates to second-order terms:

$$\dot{z} = a_0(r\Gamma(\mu) - r_0) + a_2 z^2 + O(z^3). \tag{7}$$

See Appendix A for details of the derivation of the first-order expansion for r_c given by Eq. (6).

Escape: $r > r_c(\epsilon)$. There are initial conditions for Eqs. (3) and (4) arbitrarily close to $(x_{\text{eq}}^{(\text{s},0)},0)$ that escape, following the unstable manifold of $(x_{\text{eq}}^{(\text{u},1)},1)$.

The expression for $r_c(\epsilon)$ shows that in the limit $\max\dot{\lambda} \ll \lambda_{\max}$ ($\epsilon \ll 1$, long "gentle" ramps) the critical rate $r_c(\epsilon)$ for the ramp approaches the critical rate r_0 for the linear shift from above.

The expansion Eq. (6) for the saddle-connection is determined entirely by quantities close to the saddle-node, because $x(t)$ is ϵ-close to $y^{(\text{s})}[r\Gamma(\mu)]$ for $\mu < \mu_{\text{crit}}$, and it is ϵ-close to $y^{(\text{u})}[r\Gamma(\mu)]$ for $\mu > \mu_{\text{crit}}$ (recall that Γ equals 1 only for $\mu = \mu_{\text{crit}}$).

Figure 1(b) illustrates the phase space for the example from Sec. IV in comoving coordinates (for scalar y),

$$\dot{y} = f(y) + br\Gamma(\mu), \tag{8}$$

$$\dot{\mu} = \epsilon\Gamma(\mu), \tag{9}$$

with $r = r_0$. This is an illustration of the tracking scenario with $r < r_c(\epsilon)$, where we have a connecting orbit between $(y,\mu) = (y^{(\text{s})}[0],0)$ and $(y^{(\text{s})}[0],1)$. The distance of the connecting orbit to $y^{(\text{s})}[r_0\Gamma(\mu)] \to 0$ as $\epsilon \to 0$.

The branches of equilibria $y^{(\text{s})}[r\Gamma(\mu)]$ and $y^{(\text{u})}[r\Gamma(\mu)]$ change their arrangement depending on the value of r in relation to r_0. For $r < r_0$ there exist a continuous branch of stable (unstable) equilibria connecting $y^{(\text{s})}[0]$ ($y^{(\text{u})}[0]$) between $\mu = 0$ and $\mu = 1$. For $r = r_0$, the two branches meet as depicted by Fig. 1(b). The connections then break up for $r > r_0$ such that two separate saddle-node bifurcations are formed. Appendix B contains illustrations for the phase space for other rates.

III. NOISE-INDUCED ESCAPE DURING RAMP NEAR BUT BELOW CRITICAL RATE

We consider the effect of additive noise for the scalar setting. Then, system Eqs. (3) and (4) change into a scalar stochastic differential equation (SDE) for a random variable X_t,

$$dX_t = f\left(X_t + \frac{r}{\epsilon}\mu\right)dt + \sqrt{2D}dW_t, \tag{10}$$

$$\dot{\mu} = \epsilon\Gamma(\mu), \tag{11}$$

where W_t is standard Brownian motion, the intensity of the noise is given by $\sqrt{2D}$, and D is a constant diffusion coefficient. We assume that the deterministic part is as described in Sec. II. The deterministic part in Eq. (10) corresponds to a choice of b equal to 1 in the general Eq. (3). Setting $Y_t = X_t + r\mu/\epsilon$ gives

$$dY_t = (f(Y_t) + r\Gamma(\mu(t)))dt + \sqrt{2D}dW_t \tag{12}$$

where $\dot{y} = f(y) + r\Gamma(\mu)$ follows the scenario from Sec. II when treating μ as a parameter. That is, for $r = r_0$, the system touches a saddle node nontransversally when μ crosses μ_{crit}. As introduced in Sec. II, the $y^{(\text{s})}$ and $y^{(\text{u})}$ are the stable and unstable branches. They are arranged such that $y^{(\text{s})}[r\Gamma(\mu)] < y^{(\text{u})}[r\Gamma(\mu)]$, as shown in Fig. 1(b), when $r\Gamma(\mu) \in [0,r_0)$ (consistent with our setup in Sec. II and the example in Sec. IV). This means that

$$x_{\text{eq}}^{(\text{s},0)} = y^{(\text{s})}[r\Gamma(\mu)]|_{r=0} < x_{\text{eq}}^{(\text{u},0)} = y^{(\text{u})}[r\Gamma(\mu)]|_{r=0}$$

are equilibria of the deterministic part of Eq. (10) combined with $\dot{\mu} = \epsilon\Gamma(\mu)$ [identical to Eq. (4) with the same assumptions Eq. (5) on Γ)]. Expressions below also use the potential U_r for the deterministic part of Eq. (12):

$$U_r(y) = -\int f(y)dy - r\Gamma y.$$

A. Stationary case with noise (Equation (10) with $r = 0$, which is independent of μ)

For $D > 0$ there will be a fixed escape rate κ from the basin of attraction of $x_{\text{eq}}^{(\text{s},0)}$ across $x_{\text{eq}}^{(\text{u},0)}$, approximated by Kramers' escape rate:

$$\kappa \approx \frac{\sqrt{\alpha\beta}}{2\pi}\exp\left(-\frac{\Delta U_0}{D}\right), \tag{13}$$

where $\alpha = \partial_{yy}U_0(x_{\text{eq}}^{(\text{s},0)})$, $\beta = -\partial_{yy}U_0(x_{\text{eq}}^{(\text{u},0)})$, and $\Delta U_r = U_r(y^{(\text{u})}[r]) - U_r(y^{(\text{s})}[r])$ (ΔU_0 is then ΔU_r at $r = 0$). The approximation Eq. (13) is accurate for $D \ll \Delta U_0$.

B. First-order approximations of nonstationary Fokker-Planck Equation (FPE)

We study the first-order deviation from the quasistationary escape rate for $0 < \epsilon \ll 1$. For the following section we fix a specific trajectory for $\mu(t)$ in $\dot{\mu} = \epsilon\Gamma(\mu)$ by choosing the initial condition such that

$$\mu = \mu_{\text{crit}} \quad \text{for } t = 0$$

(remember that $\Gamma(\mu_{\text{crit}}) = 1$ is the unique maximum of Γ). We are interested in the parameter range where the diffusion coefficient D and the maximal ramp speed r satisfy

$$D = O(\epsilon^{3/2}), \quad r - r_c(\epsilon) = O(\epsilon) < 0.$$

Thus, the maximal ramp speed r is close to but below its critical value $r_c(\epsilon)$ given in Eq. (6). The scaling of the diffusion coefficient arises naturally from the change of coordinates to Eq. (7) with white noise of variance $2D$; see Appendix A. For $D \ll \epsilon^{3/2}$ we have a small-noise limit for $\epsilon \to 0$ for the probability of escape, governed by Kramers' escape rate Eq. (13). For $D \gg \epsilon^{3/2}$, the probability of escape is dominated by noise-induced escape far away from the tipping. For $D \sim \epsilon^{3/2}$, all coefficients in the nondimensionalized system are of order unity such that the time-dependence and the noise effects are in nontrivial balance for all small ϵ. The scaling implies in particular that

$$0 < D \sim \Delta U_r \ll \Delta U_0. \tag{14}$$

Remarks: (*a*) Condition Eq. (14) means that the escape rate is small before and after the ramp ($t \to \pm\infty$, $\mu(t)$ far from μ_{crit}) such that the Kramers approximation Eq. (13) for the escape rate is applicable for all times outside of an interval $[t_0, T_{\text{end}}]$ around $t = 0$.

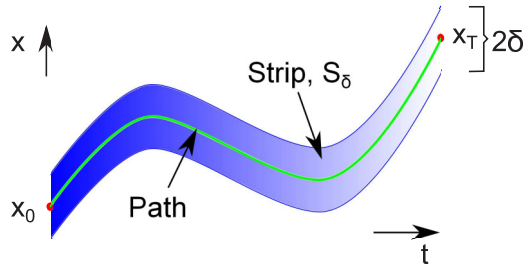

FIG. 2. Sketch of the path $\tilde{x}(t)$ (green curve) and the surrounding strip S_δ of width 2δ (shaded blue). The probability density of a realization passing through (x,t) (always staying within S_δ) is $P(x,t)$.

(b) Condition Eq. (14) also means that the maximal ramp speed r is sufficiently large such that approximation Eq. (13) is no longer true at the maximum speed of the ramp ($t = 0$, $\mu = \mu_{\text{crit}}$), but it is still less than the saddle-node rate r_0 (note that $\Delta U_{r_0} = 0$), the limit of the critical rate $r_c(\epsilon)$ for $\epsilon \to 0$. Thus, without noise ($D = 0$), there is a connection from $(x_{\text{eq}}^{(s,0)},0)$ to $(x_{\text{eq}}^{(s,1)},1)$ (the case of *tracking* in Sec. II). Let us pick one time profile $\tilde{x}(t)$ on this connecting orbit.

We consider a starting position $(x,t) = (x_0,t_0)$ and an end position at $(x,t) = (x_T,T_{\text{end}})$, and a strip S_δ of width 2δ and length $T_{\text{end}} - t_0$ around $\tilde{x}$; see Fig. 2.

The Fokker-Planck equation,

$$\frac{\partial P}{\partial t} = D\frac{\partial^2 P}{\partial x^2} - \frac{\partial}{\partial x}(f(x + r\mu(t)/\epsilon)P), \tag{15}$$

describes the time evolution of the probability density $P(x,t)$ of the random variable X_t, governed by Eq. (10). If we impose Dirichlet boundary conditions,

$$0 = P(\tilde{x}(t) + \delta,t), \tag{16}$$

$$0 = P(\tilde{x}(t) - \delta,t), \tag{17}$$

then $\int_a^e P(x,t)dx$ is the probability that the solution of Eq. (10), starting at t_0 with probability density $P(\cdot,t_0)$, is in $[a,e]$ at time t and has never left the strip S_δ.

Consequently, the overall escape probability from the strip S_δ of width 2δ around the path $\tilde{x}$ during time interval $[t_0,T_{\text{end}}]$ equals $1 - \int_{-\delta}^{\delta} P(\tilde{x}(T_{\text{end}}) + x,T_{\text{end}})dx$.

Figure 3 illustrates the shape of this probability density $P(x,t)$ along the strip S_δ for a ramp speed $r < r_c(\epsilon)$. The figure uses parameters from the specific example introduced in Sec. IV. The first moment of $P(x,t)$ (the mean) is shown in panel (a) of Fig. 3. Panels (b)–(d) show the profile of $P(x,t)$ for selected times t. The numerical solution of Eqs. (15) and (16) is shown as a blue (dashed) curve. The other curves are the approximations described below.

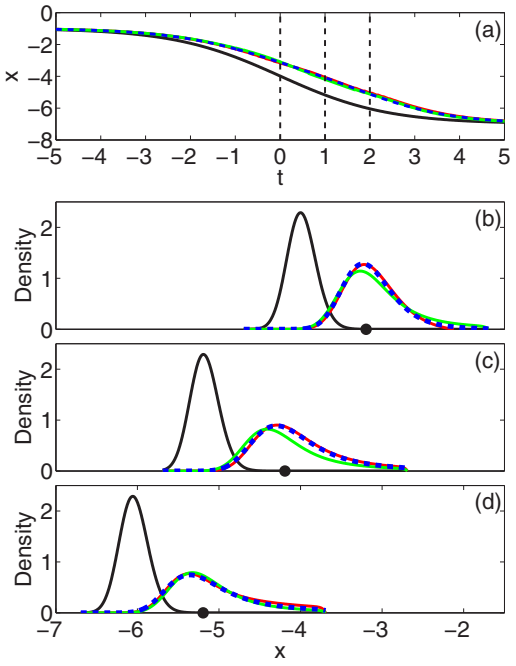

FIG. 3. Comparison of the single- [green (light gray)] and three-mode [red (dark gray)] approximations with the density from simulations (blue dashed) and stationary density (black) for $\epsilon = 0.21$, $r = 1.26$. Panel (a) provides the time profile for the location of the mean of each distribution. Vertical dashed lines indicate the times for which the densities are given in the remaining panels, namely (b) $t = 0$, (c) $t = 1$, and (d) $t = 2$. Black dot on x axis [panels (b)–(d)] corresponds to location of deterministic trajectory starting at $x_0 = -1$ at $t = -10$. Parameters: Noise level $D = 0.06$, width of strip S_δ $2\delta = 3$.

C. Uncentered quasistationary density

The crudest approximation assumes that the density is approximately stationary throughout the ramp. This implies that $\partial_t P$ is small in Eq. (15). Replacing $\partial_t P$ with zero in Eq. (15) and imposing a Dirichlet boundary condition on the right end ($P(\tilde{x}(t) + \delta,t) = 0$), the solution P of Eq. (15) has the form

$$P_*(x,t) = P_0(t)\int_x^{\tilde{x}(t)+\delta} \exp\left[\frac{U(x',t) - U(x,t)}{D}\right]dx', \tag{18}$$

where $\partial_x U(x,t) = -f(x + r\mu(t)/\epsilon)$ for each fixed t. The spatial shape of $P_*(\cdot,t)$ is nearly unchanged, only shifted by $r\mu(t)/\epsilon$ for different times t. As the density has nearly constant shape for all t, the escape rate is nearly constant in time as well [hence, it is equal to κ by remark (a)]. This escape rate determines the normalization constant $P_0(t)$: $P_0(t) \approx P_\infty(1 - (t - t_0)\kappa)$, where P_∞ is such that the initial density $P_*(x,t_0)$ has a unit integral. This approximation, shown in black in Fig. 3 for the example from Sec. IV, does not catch the effect of a nonzero r: it is (nearly) independent of r (becoming independent of r in the limit $\delta \to \infty$). The density $P_*(x,t)$ is centered at $x_{\text{eq}}^{(s,0)} - r\mu(t)/\epsilon$, which is visibly smaller than $\tilde{x}(t)$ (the location of the deterministic trajectory, highlighted by the black dot on the x axis in Figs. 3(b)–3(d)).

D. Instantaneous eigenmodes of FPE centered at $\tilde{x}$

The instantaneous eigenmode expansion for the linear operator of the Fokker-Planck Eq. (15) follows an approach similar to that presented in Risken and Frank [22], Zhang *et al.* [23] but for a time-dependent deterministic part $f(x + r\mu(t)/\epsilon)$ instead of a time-independent $f(x)$.

Figure 3 shows the single-mode approximation ($n = 1$) in green (light gray) and the three-mode approximation ($n = 3$) of the probability density in red (dark gray).

We first change to a comoving coordinate system $x = \tilde{x}(t) + y$ with respect to y, such that, the SDE Eq. (10) has the form

$$dy = -yg(y,t)dt + \sqrt{2D}dW_t, \quad \text{where} \tag{19}$$

$$g(y,t) = -\int_0^1 f'(sy + \tilde{y}(t))ds, \quad \text{with}$$

$$\tilde{y}(t) = y^{(s)}[r\Gamma(\mu(t))] - \epsilon \frac{r\Gamma'(\mu(t))\Gamma(\mu(t))}{f'(y^{(s)}[r\Gamma(\mu(t))])^2} + O(\epsilon^2)$$

(recall that $y^{(s)}[r\Gamma(\mu)]$ is the stable equilibrium of $\dot{y} = f(y) + r\Gamma(\mu)$ with fixed μ). For sufficiently small ϵ and $r < r_0$, we have that in the moving coordinates y the equilibrium $y=0$ is stable without noise for each fixed t (by the stability assumption on $y^{(s)}\{r\Gamma[\mu(t)]\}$ and because $r < r_0$). That is, for $t \in [t_0, T_{\text{end}}]$

$$g(0,t) = -f'(\tilde{y}(t)) = -f'(y^{(s)}[r\Gamma(\mu(t))]) + O(\epsilon) > 0.$$

The Fokker-Planck equation for the density $P(y,t)$ over y operates then on the fixed domain $[-\delta,\delta]$:

$$\frac{\partial P}{\partial t} = D\frac{\partial^2 P}{\partial y^2} + \frac{\partial}{\partial y}[yg(y,t)P] =: A(t)P, \tag{20}$$

with Dirichlet boundary conditions $P(-\delta,t) = P(\delta,t) = 0$. The operator $A(t)$ is self-adjoint with respect to the scalar product

$$\langle w,v\rangle_t = \int_{-\delta}^{\delta} w(y)v(y)\exp\left[\frac{U(y,t)}{D}\right]dy, \tag{21}$$

where U is the potential corresponding to the drift $-yg(y,t)$ ($\partial_y U(y,t) = yg(y,t)$). Since $g(y,t) > 0$, this effective potential $U(y,t)$ has a critical point at $y = 0$. For each fixed $t \in [t_0, T_{\text{end}}]$, the spectrum of $A(t)$, shown later in Fig. 5 for the specific example considered in Sec. IV, consists of eigenvalues $\gamma_i(t)$ with eigenfunctions $v_i(y,t)$:

$$\gamma_i v_i = D\frac{\partial^2 v_i}{\partial y^2} + \frac{\partial}{\partial y}[yg(y,t)v_i] = A(t)v_i. \tag{22}$$

The eigenfunctions $v_i(\cdot,t)$ (called *instantaneous* modes as they are time-dependent) form an orthonormal basis of L^2 with respect to $\langle\cdot,\cdot\rangle_t$. Thus, we can expand the solution $P(y,t)$ of Eq. (20) as a linear combination of the instantaneous eigenmodes v_i:

$$P(y,t) = \sum_{i=1}^{\infty} a_i(t)v_i(y,t), \tag{23}$$

where the $a_i(t)$ are scalar coefficients at each time t.

Inserting the expansion Eq. (23) into Eq. (20), applying $\langle v_k,\cdot\rangle_t$, and truncating at a finite n, gives [24]

$$\dot{a}_k = \gamma_k(t)a_k(t) - \sum_{i=1}^{n}\langle v_k(t),\dot{v}_i(t)\rangle_t a_i(t), \tag{24}$$

$$a_i(0) = \langle v_i(\cdot,0), P(\cdot,0)\rangle_0,$$

where the coupling coefficients $\langle v_k(t),\dot{v}_i(t)\rangle_t$ are of order $\epsilon/|\gamma_k(t) - \gamma_i(t)|$ for $i \neq k$. Thus, the sum is convergent and the truncated solution

$$P_n(x,t) = \sum_{i=1}^{n} a_i(t)v_i(x,t) \tag{25}$$

converges to P for $n \to \infty$ and for $\epsilon \to 0$ [$-\gamma_k = O(k^2)$ for positive D (see Fig. 5(a) for the specific example), so, in particular, $P_n - P = O(\epsilon)$].

Since the initial t_0 is such that $\mu(t_0)$ is still close to 0, $\gamma_1(t_0)$ will be very close to zero by remark (a) that escape is unlikely outside of the ramping time interval. Remark (a) also implies that the coefficients of the initial value $P(\cdot,t_0)$, $a_i(t_0)$, are close to zero for $i > 1$.

Figure 3 illustrates that the truncation error for small n occurs in the tails of the distribution. For example, for the single-mode approximation with $n = 1$, Eq. (24) simplifies to

$$\dot{a}_1 = [\gamma_1 - \langle v_1,\dot{v}_1\rangle_t]a_1.$$

Ignoring the $O(\epsilon)$ term $\langle v_1,\dot{v}_1\rangle_t$, the single-mode approximation results in an approximate solution

$$P_1(y,t) = \exp\left(\int_{t_0}^{T_{\text{end}}}\gamma_1 dt\right)v_1(y,t).$$

Thus, truncation at $n = 1$ assumes that the density instantaneously adjusts its shape to the shape of the effective potential well $U(y,t) = -\int yg(y,t)dy$ at every time t.

For each particular truncation n, the probability $\mathbb{P}_M$ for the trajectory of a realization to not remain within the strip S_δ is approximately

$$\mathbb{P}_M = 1 - \int_{-\delta}^{\delta} P_n(y,T_{\text{end}})\,dy. \tag{26}$$

E. Perturbation approximation of the dominant eigenvalue

The dominant eigenvalue $\gamma_1(t)$ and eigenfunction v_1 can be approximated via a linear perturbation analysis from the small-noise limit ($D \to 0$). Hence, we can approximate the dominant term in $\mathbb{P}_M$ for the truncation $n = 1$, which is accurate to order ϵ. Consider again the eigenvalue problem for the Fokker-Planck equation:

$$\gamma(t)P(y,t) = D\frac{\partial^2 P(y,t)}{\partial y^2} + \frac{\partial}{\partial y}[U'(y,t)P(y,t)], \tag{27}$$

for $y \in (a,\delta)$ (where a can be $-\infty$ in some expressions below, but we will finally set $a = -\delta$). We now consider t simply as a parameter in the eigenvalue problem (such that eigenvalue γ and eigenfunction P depend on the parameter t since the coefficient U' depends on t). We will drop this parameter t throughout this subsection. The basic building block of solutions of Eq. (27) is the function $\exp(-U(y)/D)$, which we call

$$p(y) = \exp(-U(y)/D), \tag{28}$$

along with antiderivatives of products of p of various orders, which we call

$$p_{s_1\ldots s_k}(y_0) = \int_{y_0}^{\delta} \ldots \int_{y_{k-1}}^{\delta} \exp\left[\sum_{j=1}^{k} \frac{(-1)^{s_j} U(y_j)}{D}\right] dy_k \ldots dy_1$$

(the subscripts s_j will be 1 or 2). We know that

$$\gamma = 0, \quad P_*(y) = p(y)p_2(y)/p_{12}(a) \tag{29}$$

solve Eq. (27) with the two boundary/integral conditions

$$P(\delta) = 0, \quad \int_a^{\delta} P(y)dy = 1. \tag{30}$$

The expression for P_* in Eq. (29), equals Eq. (18) for P_* with the specific normalization constant $P_0 = J/D$, where J represents the probability flux. The probability flux J is the flow of probability per unit time per unit area.

The integral condition in Eq. (30) is based on an assumption that is only approximately correct if the noise level D is small: the probability flux J is constant in y such that the flux through the right boundary at $+\delta$ must also enter at $y = -\infty$ such that J is given by

$$J = \frac{D}{p_{12}(a)}. \tag{31}$$

The more appropriate boundary conditions for nonsmall noise level D result in the eigenvalue problem Eq. (27) for γ and P, with

$$P(a) = 0, \quad P(\delta) = 0, \quad \int_a^{\delta} P(y)dy = 1,$$

which leads to a uniformly non-zero γ, including for the limit $a \to -\infty$.

We can express a first-order approximation of γ for nonsmall noise in terms of p, given in Eq. (28), by treating it as a perturbation of the small-noise limit and of $\gamma = 0$, $P = P_*$. For a finite $a \ll -1$ let us introduce the value of the solution P of Eq. (27) at a as a parameter π_a:

$$P(a) = \pi_a. \tag{32}$$

Then, we get a solution pair (γ, P) of Eq. (27) with boundary conditions Eqs. (30) and (32) for each small π_a. For $\pi_a = P_*(a) = p(a)p_2(a)/p_{12}(a)$, the solution is $\gamma = 0$, $P = P_*$. So, to first order in π_a, we have for the parameter $\pi_a = 0$,

$$\gamma \approx -\gamma' P_*(a) = -\gamma' \frac{p(a)p_2(a)}{p_{12}(a)} \quad \text{with} \quad \gamma' = \left.\frac{d\gamma}{d\pi_a}\right|_{\pi_a = P_*(a)}. \tag{33}$$

The scalar γ' is part of the solution pair (γ', q) of the linearization of eigenvalue problem Eq. (27) with boundary conditions Eqs. (30) and (32), with respect to π_a in $\pi_a = P_*(a)$, $P = P_*$, $\gamma = 0$:

$$\gamma' P_* = \frac{\partial}{\partial y}\left[D\frac{\partial q}{\partial y} + U'(y)q\right], \tag{34}$$

with conditions

$$q(a) = 1, \quad q(\delta) = 0, \quad \int_a^{\delta} q(y)dy = 0.$$

This is an affine equation for γ' and q, which can be solved by integration, resulting in

$$\gamma' = \frac{Dp_{12}(a)^2}{p(a)[p_{12}(a)p_{212}(a) - p_2(a)p_{1212}(a)]},$$

such that the first-order estimate Eq. (33) gives

$$\gamma_1 := \gamma \approx \frac{D}{\frac{p_{1212}(a)}{p_{12}(a)} - \frac{p_{212}(a)}{p_2(a)}}. \tag{35}$$

Taking into account now that all quantities in Eq. (35) depend parametrically on time t, the probability $\mathbb{P}_P$ of not following a path within a specific region is approximately

$$\mathbb{P}_P = 1 - \exp\left[\int_{t_0}^{T_{\text{end}}} \gamma_1(t)dt\right], \tag{36}$$

where γ_1 is given approximately in Eq. (35), when inserting $-\delta$ for a. We can compare Eq. (36) with the simpler probability formula $\mathbb{P}_J$, which is valid in the small noise limit

$$\mathbb{P}_J = 1 - \exp\left[-\int_{t_0}^{T_{\text{end}}} J(t)\,dt\right], \tag{37}$$

where the probability flux J is given in Eq. (31), when again inserting $-\delta$ for a.

Section V will compare Monte-Carlo simulations, the numerical approximation using the first n instantaneous eigenmodes of the linear operator $A(t)$ of the Fokker-Planck equation, the perturbation formula for the leading eigenvalue $\gamma_1(t)$, and the formula for the probability flux $J = D/p_{12}(a)$ for the stationary density P_* in Eq. (29), which is accurate for small escape rates.

IV. SADDLE-NODE NORMAL FORM WITH PARAMETER RAMP AND NOISE

A prototypical model for rate-induced tipping was introduced by Ashwin *et al.* [5]. The time evolution of a scalar dependent variable $x(t) \in \mathbb{R}$ is described by the saddle-node normal form equation:

$$\dot{x} = f(x,\lambda) = (x + \lambda)^2 - 1, \tag{38}$$

where, without loss of generality, we have set the normal form parameter to equal 1. The ODE Eq. (38) has two families of equilibria; one stable family $W^{(s)}[0] = -\lambda - 1$ and one unstable family $W^{(u)}[0] = -\lambda + 1$. The parameter λ in Eq. (38) is assumed to be time dependent following a ramp given by

$$\lambda(t) = \frac{\lambda_{\max}}{2}\left[\tanh\left(\frac{\lambda_{\max}\rho t}{2}\right) + 1\right], \tag{39}$$

where $\lambda_{\max}$ determines how far the parameter λ is shifted and ρ adjusts the speed of the ramp. Equation (39) can be described by an ODE for λ with the condition $\lambda(0) = \lambda_{\max}/2$. Therefore, the prototypical model can be described by the two

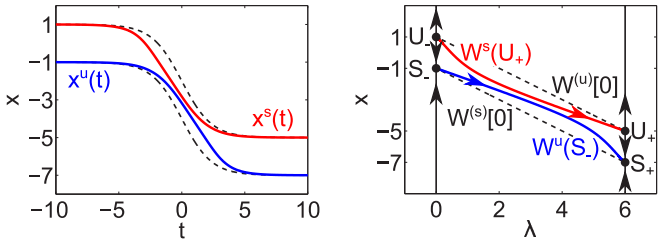

(a) (b)

FIG. 4. Time profile (a) and phase plane (b) of system Eqs. (40) and (41) for $\rho = 0.14 < \rho_c$. Black dashed curves are the stable ($W^{(s)}[0] = -1 - \lambda$) and unstable ($W^{(u)}[0] = 1 - \lambda$) branches of equilibria in the limit $\rho = 0$, blue and red curves are the unstable and stable manifolds, $W^u(S_-)$ and $W^s(U_+)$, respectively ($\lambda_{\max} = 6$).

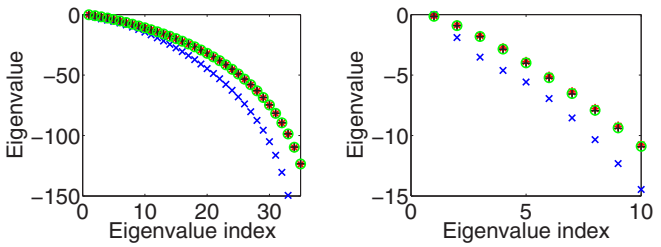

(a) (b)

FIG. 5. Eigenvalue spectrum of the linear operator $A(t)$ for the Fokker-Planck equation corresponding to the system Eqs. (40) and (41), with $\rho = 0.14$ ($\epsilon = 0.21$, $r = 1.26$), $D = 0.06$ and at times $t = -10$ (blue cross), $t = 0$ (red star), $t = 1$ (black plus), and $t = 2$ (green circle).

dimensional ODE in the (x,λ) phase plane,

$$\dot{x} = (x + \lambda)^2 - 1, \tag{40}$$

$$\dot{\lambda} = \rho\lambda(\lambda_{\max} - \lambda). \tag{41}$$

For this system of ODEs a critical speed $\rho = \rho_c = 4/[\lambda_{\max}(\lambda_{\max} - 2)]$ was found in Ref. [25], at which a heteroclinic connection $(x,\lambda) = (-1 + (2/\lambda_{\max} - 1)\lambda, \lambda)$ from $(-1,0)$ to $(1 - \lambda_{\max}, \lambda_{\max})$ occurs (setting the critical rate ρ_c for rate-induced tipping). The time profile and phase portrait for $\rho < \rho_c$ is presented in Fig. 4. For a complete overview of all possible time profiles and phase portraits, see Ritchie and Sieber [10].

System Eqs. (40) and (41) have four equilibria: two saddles $S_- = (-1,0)$, $U_+ = (-5,6)$, one stable node $S_+ = (-7,6)$, and one unstable node $U_- = (1,0)$; see Fig. 4(b). The dashed lines $W^{(s)}[0] = -1 - \lambda$ and $W^{(u)}[0] = 1 - \lambda$ represent the family of stable and unstable equilibria for $\rho = 0$, respectively. The curve $W^u(S_-)$ is the unstable manifold of the saddle S_- and $W^s(U_+)$ is the stable manifold of the saddle U_+. The time profile for x on the invariant manifolds $W^u(S_-)$ and $W^s(U_+)$, denoted $x^u(t)$ and $x^s(t)$, respectively, is given in Fig. 4(a).

The manifold $W^s(U_+)$ acts as a separatrix partitioning the plane into two distinct regions. Below $W^s(U_+)$ all trajectories are attracted towards the stable node S_+, while any trajectories above the separatrix escape to $+\infty$ in finite time.

We will continue using the parameters ρ and $\lambda_{\max}$ to remain consistent with the studies of Refs. [5,10,25]. The parameters ρ and $\lambda_{\max}$ (both are nonsmall) have the following relation to the parameters ϵ and r of Secs. II and III:

$$\epsilon = \frac{\rho\lambda_{\max}}{4}, \quad r = \frac{\rho\lambda_{\max}^2}{4}, \quad \lambda_{\max} = \frac{r}{\epsilon}, \quad \rho = \frac{4\epsilon^2}{r}.$$

Using r and ϵ, system Eqs. (40) and (41) have the form

$$\dot{x} = (x + r\mu/\epsilon)^2 - 1, \quad \dot{\mu} = 4\epsilon\mu(1 - \mu),$$

the critical rate is $r_c(\epsilon) = 1 + 2\epsilon$, and the connecting orbit has the form $(x,\mu) = [-1 + \mu(2 - r/\epsilon), \mu]$. We will keep $\lambda_{\max} = 6$ fixed and vary ρ between 0 and 1/6, which simultaneously varies ϵ between 0 and 0.25 and r between 0 and 1.5. Therefore, we will always have $\epsilon \ll 1$ corresponding to gentle but long ramps.

The dynamics of x for the system Eqs. (40) and (41), modified by adding noise to Eq. (40), are described by a stochastic differential equation [an example of the general Eq. (10)]:

$$dX_t = [(X_t + \lambda(t))^2 - 1]dt + \sqrt{2D}dW_t. \tag{42}$$

The expressions [for example, Eq. (36)] for probability of escape refer to a strip of half-width δ around a deterministic reference trajectory $\tilde{x}(t)$. We choose the trajectory $x^u(t)$ [blue curve in Fig. 4(a) on the unstable manifold $W^u(S_-)$] and a strip with a fixed width $2\delta = 3$ around $\tilde{x}(t)$. Then we use the approximations for $\mathbb{P}$, Eqs. (26), (36), and (37), derived in Sec. III, to find the probability of escape.

As described in Sec. III, we use comoving coordinates,

$$y(t) = x(t) - x^u(t),$$

such that the domain for y, $[-\delta,\delta]$ is fixed for all t. This transformation alters the ODE given in Eq. (40):

$$\begin{aligned} \dot{x} &= f(x,\lambda) = (x + \lambda)^2 - 1, \\ \dot{y} + \dot{x}^u &= f(y + x^u, \mu), \\ \dot{y} &= (y + x^u + \lambda)^2 - 1 - \dot{x}^u, \\ &= y^2 + \underbrace{2(x^u + \lambda)}_{-c_1(t)} y + \underbrace{(x^u + \lambda)^2 - 1 - \dot{x}^u}_{\text{equals } 0}, \end{aligned} \tag{43}$$

and so, instead of Eq. (40), we can express the new ODE as

$$\dot{y}(t) = yg(y(t),t) = y^2(t) - c_1(t)y(t), \tag{44}$$

where $c_1(t)$ is a time-dependent scalar. Thus, $yg(y,\mu(t))$ is used in the eigenvalue problem of the Fokker-Planck Eq. (27), with Dirichlet boundary conditions:

$$P(-\delta,t) = P(\delta,t) = 0.$$

Figure 5(a) gives the spectrum of the eigenvalues for different fixed times t and for noise level $D = 0.06$. The eigenvalues for the times when the system Eqs. (40) and (41) is close to stationary (roughly all $t \notin [-3,3]$), is given in blue. The eigenvalues during the ramp (when $\dot{\lambda}$ is of order 1) are given by the other colors, namely at $t = 0$ (red star), $t = 1$ (black plus) and $t = 2$ (green circle). All sets of eigenvalues γ_k are on parabolas ($\gamma_k = \mathrm{Re}\gamma_k \sim -k^2$) [Fig. 5(a)], with a nearly

linear relationship $\gamma_k \sim -k$ for the dominant eigenvalues [Fig. 5(b)] and $\gamma_1(t) \approx 0$ for all t.

Notice, that the first three eigenvalues during the ramp are all greater than the second eigenvalue for times when the system is close to stationary, for example, at $t = -10$ (blue). Thus, the contribution of additional modes is more significant during the period of the shift. The computational study in Sec. V will compare single- and three-mode approximations.

We return to Fig. 3, which displays different types of densities to be compared with the reference probability density from simulations in blue. We will focus on the comparison between the single- [green (light gray)] and three-mode approximations [red (dark gray)] to the reference probability density for ramping speed $\rho = 0.14$ ($\epsilon = 0.21$, $r = 1.26$). According to our analysis all differences between approximations and simulation results are caused by the nonzero ϵ.

Initially, both the single-mode and three-mode approximation match the probability density well (not shown); however, a visible deviation appears in the single-mode at $t = 0$; see Fig. 3(b). The single-mode approximation develops a larger tail than the density from simulations (and the three-mode approximation). This corresponds to an overestimation of the escape and hence, the peak of the density is lower. The density has also shifted further along the x axis because the density instantaneously adjusts to the effective potential, as previously discussed. In contrast the three-mode approximation is still providing a good match to the reference probability density. For larger times the single-mode is underestimating the escape compared to the simulations. The single-mode approximation converges back to the reference density for $t > 2$ [Fig. 3(d)] when the shift slows down. The three-mode approximation follows the reference density with greater accuracy throughout.

V. SYSTEMATIC PARAMETER STUDY IN ρ AND D

In this section, we will compare different approximations for the probability of escape (noise and rate-induced tipping) in the two parameter (ρ, D) plane. We will use Monte Carlo simulations (described below) as the reference for the probability of escape. Section III proposed two approximate expressions for the single-mode approximation:

(a) the escape probability based on the probability flux $J = D/p_{12}(a)$ with $a = -\delta$, given in Eq. (37);

(b) the escape probability based on the first-order approximation of the leading eigenvalue γ_1, given in Eq. (36) (also with $a = -\delta$).

We also compute the escape probabilities based on single- and three-mode approximations, by solving the ODE eigenvalue problem Eq. (27) with Dirichlet boundary conditions at $-\delta$ and δ numerically for the first n modes $((\gamma_k, v_k), k = 1, \ldots, n)$ together with the ODE Eq. (24), such that the escape probability is given by Eq. (26) for $n = 1$ and $n = 3$.

Figure 6(a) shows the probability of noise and rate-induced tipping occurring in the two parameter (ρ, D) plane, calculated using Monte Carlo simulations. This has been performed by starting with a large number of realizations at $x_0 = -1$ at $t_0 = -10$ and evolving according to the SDE Eq. (10). The fraction of realizations that pass $x_T = 4$, and, hence, go to $+\infty$ in finite time, approximates the probability of tipping (or probability of escape). The reference probability is not derived

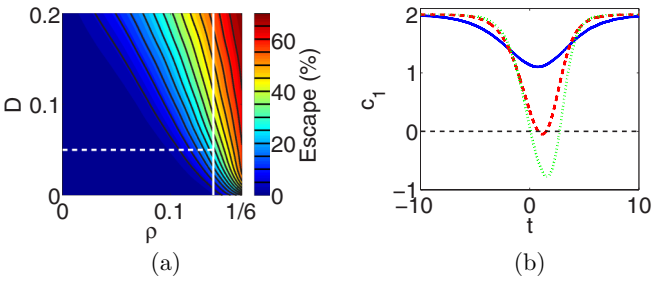

FIG. 6. (a) Overview probability of escape in the (ρ, D) plane using simulations (with smoothing), where contours are spaced for every 5% of escape. Vertical white line indicates value of ρ such that $\min(c_1) = 0$ and horizontal dashed line shows lowest value of D for which the probability can be calculated for the modes. (b) Time profile of the critical points of $U(y,t)$, one of them is always $y = 0$, the other is $c_1(t)$ for $\rho = 0.08$ (blue solid), 0.14 (red dashed), and 0.16 (green dotted).

from the number of realizations escaping the strip $\{y(t) \in [-\delta, \delta] : t \in [t_0, T_{\text{end}}]\}$ but by the fraction of realizations that have crossed an arbitrary line $x_T = 4$ (the choice of δ and x_T is such that this difference has a small effect).

Figure 6(a) shows the probability of escape (in %) for all ramping speeds ρ up to $\rho_c = 1/6$ and a range of noise levels D. The color contours indicate that the probability of escape is small for small ρ and D. As ρ increases towards ρ_c and the noise level increases so does the probability of escape, reaching approximately 70% probability of escape for $\rho = \rho_c$ and $D = 0.2$.

A. Region in (ρ, D) plane considered

We can expect the single-mode (or three-mode) approximations to be accurate only in a range of parameters ρ up to a value $\rho_{\max} = 0.14$ that is slightly smaller than the critical value $\rho_c = 1/6$ (where tipping occurs without noise). The reason for this is in the error terms when replacing the dynamic Fokker-Planck equation for the density with its projection onto leading time-dependent mode(s). These error terms are only small if the time derivative of the (time-dependent) drift $yg(y,t)$ in Eq. (20) is small.

As introduced in Eq. (19) in Sec. III B, the eigenvalue problem for the Fokker-Planck equation is solved in a comoving coordinate system along the path $\tilde{x}(t)$ ($y = x - \tilde{x}(t)$), such that the path is centered at $y = 0$ within the fixed domain $y \in [-\delta, \delta]$ and the drift is given by $yg(y,t) = y(y - c_1(t))$ [where $c_1(t)$ is given in Eq. (43)]. Its potential $U(y,t) = -\int y(y - c_1(t))dy$ has a well at $y = 0$ and a hill top at c_1 for $c_1 > 0$, but a hill top at $y = 0$ (and a well at c_1) for $c_1 < 0$. Figure 6(b) illustrates the time profile of $c_1(t)$ for different values of the drift speed ρ. The limit of $c_1(t)$ for $t \to \pm\infty$ is 2 such that $c_1(t) \approx 2$ for t close to $t_0 = -10$ and $T_{\text{end}} = 10$. For small drift speeds ρ the deviations of c_1 from its asymptotic value are small [blue solid curve in Fig. 6(b)], while for $\rho = 0.16$ $c_1(t)$ becomes negative for some time interval, making the trajectory $x(t) = \tilde{x}(t)$ or $y(t) = 0$ locally repelling [green dotted curve in Fig. 6(b)].

The error of the single-mode approximation is small if $|\dot{c}_1(t)|$ is small, which is the case for t near t_0 and T_{end}, and for t close to the minimum of c_1. If $c_1(t) > 0$ for all t then the time

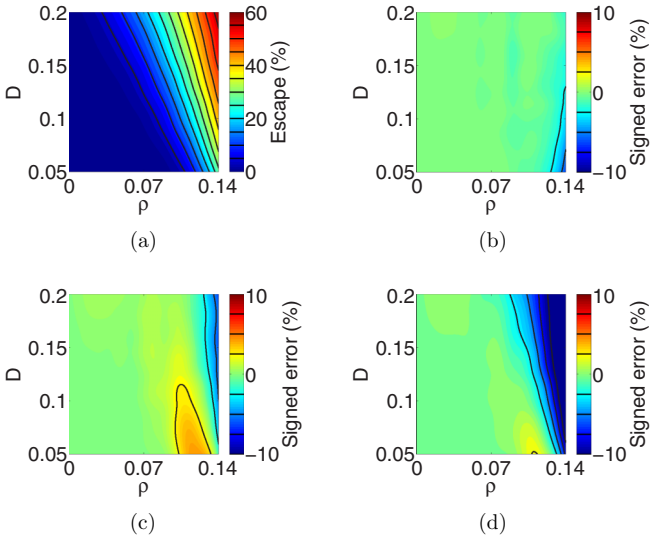

FIG. 7. (a) Reference probability of escape in (ρ, D) parameter plane, obtained using Monte Carlo simulations (with smoothing)—observing the fraction of realizations that escape the potential landscape. (b)–(d) Evaluating approximation methods for probability of escape by plotting in color the signed error % between the approximation and the reference escape. Positive error (red) reflects an overestimation and negative (blue) an underestimation. Approximation methods used: (b) Numerically calculate first three ($n = 3$) modes of the linear operator of the Fokker-Planck Eq. (26). (c) Analytical single-mode approximation Eq. (36) and (d) analytical probability flux approximation Eq. (37). Contours are spaced at 5% intervals for panel (a) and 2.5% intervals for panels (b)–(d) with the zero contour omitted.

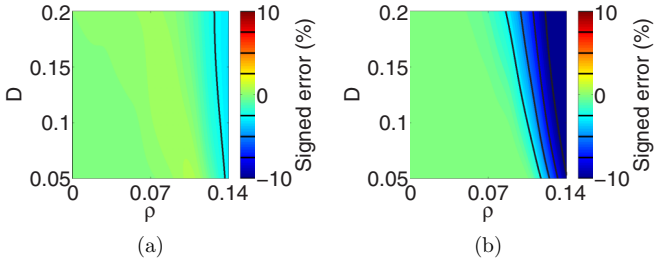

FIG. 8. Color plots of the signed error between the probability calculated numerically from the ($n = 1$) single-mode Eq. (26) and (a) the single-mode approximation Eq. (36) or (b) the probability flux approximation Eq. (37). A positive error (red) corresponds to the prescribed approximation overestimating the numerical probability calculated from the single-mode, whereas a negative error (blue) represents an underestimation. Contours are spaced at 2.5% intervals with the zero contour omitted.

$t_{\min}$, when $c_1(t)$ is minimal, correspond to those times where escape is most likely to occur, since at these times the potential barrier is smallest. At times near $t_{\min}$ the mode approximation error is also small since $|\dot{c}_1(t)|$ is small.

However, if $c_1(t) < 0$ for a range of t then escape occurs with a nonsmall probability at times when $|\dot{c}_1(t)|$ is not small, leading to an error in the single-mode approximation that is not small.

Hence, we choose a range for the parameter ρ such that $c_1(t)$ stays positive along the entire path for all ρ.

We also remove small values of D ($D < 0.05$) from our consideration, since for $\rho < \rho_c$, but not close to ρ_c, escape probabilities are small compared to errors in Monte Carlo simulations and in the numerical computations of the integrals needed for γ_1 in Eq. (35). In this region the probability of escape is exponentially small in D [that is, of order $\exp(-C/D)$ for some constant $C > 0$].

Figure 7(a) shows the reference probability—the probability of escape calculated using Monte Carlo simulations for this restricted region [with a slightly different color scale to Fig. 6(a)]. The remaining three panels of Fig. 7 give the signed error of the approximation, compared to the reference, in percent. In the color scale for these panels, a green (light gray) color represents good agreement between the approximation and reference escape. A positive error (red) means an overestimation and a negative error (blue) corresponds to an underestimation when using the approximation method.

Figure 7(b) shows the probability of escape calculated using Eq. (26) with the first $n = 3$ instantaneous eigenmodes of the linear operator of the Fokker-Planck equation. The three-mode approximation was computed by solving the ODE eigenvalue problem Eq. (22) numerically. It approximates the reference probability of escape over the specified region well, except for ρ close to 0.14 and small noise levels.

Figures 7(c) and 7(d) compare the single-mode approximation Eq. (36) and the approximation using the probability flux Eq. (37) to the reference escape. The single-mode approximation offers a very good agreement with the reference escape for $\rho < 0.1$. For larger ρ the formula gives an overestimation of the escape for small noise levels. The probability flux again approximates the probability for small ρ values well, but when the probability of escape increases to above 20% the probability flux underestimates the reference escape.

Figure 8(a) compares the single-mode approximation formula (36) to the exact single-mode approximation, solving Eqs. (22) and (26) for $n = 1$ numerically. We see that the difference is much smaller than the error caused by the approximation of the Fokker-Planck equation with a single mode; see Fig. 7(c).

In contrast, the probability flux Eq. (37) systematically underestimates the escape probability when it is greater than 20%; see Fig. 8(b). This is as expected because the estimate Eq. (37) based on a spatially constant probability flux assumes the flux escaping at the boundary $+\delta$ re-enters at the boundary $-\delta$. The difference between the two estimates is larger when the escape probability is high, because the assumption of spatially constant flux is only approximately true if escape is sufficiently rare compared to the time it takes for realizations to reach the potential well from the boundary at $-\delta$. This leads to an underestimate for those values of D and ρ when the probability of escape is greatest.

VI. DISCUSSION

We have provided approximations for the critical rate for deterministic rate-induced tipping and for the probability of noise-induced tipping during parameter shifts. These approximations are valid for parameter shifts that are asymptotic to

constant parameter values for $t \to \pm\infty$ and that are "long but gentle": the small parameter ϵ is the ratio between maximal ramp (shift) speed r and the length of the parameter shift. The deterministic critical rate $r_c(\epsilon) = r_0 + \epsilon r_1 + O(\epsilon^2)$ is an order-ϵ perturbation from the critical rate r_0 for constant-speed parameter shifts (which were discussed in Ref. [5]).

The approximation for the tipping probability in the presence of noise is based on the instantaneous eigenmode expansion of the linear operator for the Fokker-Planck equation to approximate the quasi-stationary probability densities in a strip S_δ of half-width δ around the deterministic trajectory (a connecting orbit between equilibria). Moreover, we have derived a general perturbation formula to calculate the leading eigenvalue, which approximates the probability calculated from a single eigenvalue (the single-mode approximation) and thus, gives a good approximation to the reference probability of tipping for small ϵ.

The limitation of the proposed estimate using single-mode approximation is that it fails for some maximal ramp speeds r less than r_c, even for small noise levels D. A brief derivation in Appendix A shows that the single-mode approximation is generally valid for parameters up to $r = r_0 + \epsilon r_1/2$ such that the escape rate from the strip S_δ is maximal during times when the time-derivative of the shape of the underlying potential well is minimal.

ACKNOWLEDGMENTS

P.D.L.R.'s research was supported by funding from the EPSRC Grant No. EP/M008495/1, J.S. gratefully acknowledges the financial support of the EPSRC via Grants No. EP/N023544/1 and No. EP/N014391/1. J.S. has also received funding from the European Union's Horizon 2020 research and innovation programme under Grant Agreement No. 643073.

APPENDIX A: EXPANSION OF THE CRITICAL RATE IN THE SMALL PARAMETER

This section presents in more detail the expansion of the critical rate for systems with a ramped parameter shift. The critical rate is defined as the threshold at which a system fails to track the continuously changing quasisteady state and thus generating rate-induced tipping.

The simplest example of rate-induced tipping is a system subjected to a linear parameter shift r_{lin}, $\dot{x} = f(x + b\lambda)$ with $\lambda = r_{\text{lin}} t$. We assume that the linearly shifted system ($y = x + b\lambda$),

$$\dot{y} = f(y) + r_{\text{lin}} b \tag{A1}$$

($f : \mathbb{R}^n \mapsto \mathbb{R}^n$, $y(t) \in \mathbb{R}^n$), has a generic saddle-node bifurcation at $r_{\text{lin}} = r_0 > 0$, $y = y_0$. We assume that the number of unstable dimensions of the equilibria changes from 0 to 1 at the saddle-node and that the equilibria exist for $r_{\text{lin}} < r_0$. In this section we derive the first-order expansion of the critical rate r_c in ϵ for the system

$$\dot{y} = f(y) + b(r\Gamma(\mu) - r_0), \quad \dot{\mu} = \epsilon\Gamma(\mu). \tag{A2}$$

System Eq. (A2) describes the scenario of a ramped shift $\dot{x} = f(x + br\mu/\epsilon)$ with maximal speed r, again in shifted coordinates $y = x + br\mu/\epsilon$. The direction of the shift is determined by $b \in \mathbb{R}^n$ and $\Gamma(\mu)$ satisfies the following properties:

$$\begin{aligned}
&0 = \Gamma(0) = \Gamma(1),\\
&1 = \Gamma(\mu_{\text{crit}}) = \max\{\Gamma(\mu) : \mu \in [0,1]\}, \quad \text{(this defines } \mu_{\text{crit}}),\\
&0 > \Gamma''(\mu_{\text{crit}}), \quad \text{(let } g_2 := -\Gamma''(\mu_{\text{crit}})/2),\\
&\Gamma(\mu) \in (0,1) \text{ for all } \mu \in (0,\mu_{\text{crit}}) \quad \text{and} \quad \mu \in (\mu_{\text{crit}},1),
\end{aligned} \tag{A3}$$

such that Γ has a unique nondegenerate maximum at μ_{crit}. We make a change of coordinates $y = y_0 + v_0 z$ to shift the origin in Eq. (A2) to the saddle-node bifurcation at $y = y_0$:

$$v_0\dot{z} = f(y_0 + v_0 z) + b(r\Gamma(\mu) - r_0), \tag{A4}$$

where v_0 is the right nullvector of $\partial f(y_0)$ [which has a one-dimensional nullspace by the assumption of a saddle-node bifurcation at $y = y_0$ for Eq. (A1)]. Furthermore, this assumption implies

$$f(y_0 + v_0 z) = \tfrac{1}{2} z^2 \partial^2 f(y_0) v_0^2 + O(z)^3. \tag{A5}$$

Inserting Eq. (A5) into Eq. (A4) and applying w_0^T (the left nullvector of $\partial f(y_0)$, scaled such that $w_0^T v_0 = 1$) to Eq. (A4) gives

$$\dot{z} = a_0(r\Gamma(\mu) - r_0) + a_2 z^2 + O(z)^3,$$

where $a_0 = w_0^T b$, $a_2 = \frac{1}{2} w_0^T \partial^2 f(y_0) v_0^2$ are both nonzero by the assumption of a generic saddle-node. As we assume that the equilibria for fixed μ exist for $r\Gamma(\mu) < r_0$, we can choose the orientation of v_0 such that $a_0 > 0$ and $a_2 > 0$. Thus, the reduced autonomous system Eq. (A2) has the form (for small $z \in \mathbb{R}$)

$$\dot{z} = a_0(r\Gamma(\mu) - r_0) + a_2 z^2 + O(z^3), \tag{A6}$$

$$\dot{\mu} = \epsilon\Gamma(\mu). \tag{A7}$$

We zoom into the neighborhood of the maximal rate of change of $\Gamma(\mu)$ (at μ_{crit}), $z = 0$ and $r = r_0$ by introducing rescaled variables and time:

$$\begin{aligned}
\mu_{\text{old}} &= \mu_{\text{crit}} + \sqrt{\epsilon c_m}\mu_{\text{new}}, \quad &&\text{where} \quad c_m = [g_2 r_0 a_0 a_2]^{-1/2},\\
z_{\text{old}} &= \sqrt{\epsilon c_z} z_{\text{new}}, \quad &&\text{where} \quad c_z = \left[g_2 r_0 a_0 / a_2^3\right]^{1/2},\\
r_{\text{old}} &= r_0 + \epsilon c_r r_{\text{new}}, \quad &&\text{where} \quad c_r = [g_2 r_0/(a_0 a_2)]^{1/2},\\
t_{\text{old}} &= \sqrt{c_t/\epsilon}\, t_{\text{new}}, \quad &&\text{where} \quad c_t = [g_2 r_0 a_0 a_2]^{-1/2},
\end{aligned}$$

and expanding $\Gamma(\mu)$ near its unique maximum in μ_{crit} (recall from Eq. (A3) that $\Gamma(\mu_{\text{crit}}) = 1$ and g_2 is defined as $-\Gamma''(\mu_{\text{crit}})/2$):

$$\Gamma(\mu_{\text{old}}) = \Gamma(\mu_{\text{crit}} + \sqrt{\epsilon c_m}\mu_{\text{new}}) = 1 - \epsilon g_2 c_m \mu_{\text{new}}^2 + o(\epsilon).$$

In these coordinates the extended system Eqs. (A6) and (A7) can then be written as

$$\dot{z} = z^2 + r - \mu^2 + o(1), \tag{A8}$$

$$\dot{\mu} = 1 + O(\epsilon) \tag{A9}$$

Orbits that stay close to the family of equilibria of Eq. (A1) uniformly for all $\epsilon \to 0$ are perturbations of orbits that exist for all time in the limiting system of Eqs. (A8) and (A9) for $\epsilon = 0$. We have three cases for Eqs. (A8) and (A9) with $\epsilon = 0$. In all three cases there exists a unique *globally defined* orbit $z(\mu)$ that exists for all times.

$r < 1$ (Tracking): the globally defined orbit $z(\mu)$ has the limiting behavior $z(\mu) + |\mu| \to 0$ for $\mu \to \pm\infty$ and is stable forward in time. All orbits starting with $z < 0$ and $\mu \ll -1$ converge to the globally defined orbit.

$r = 1$ (Critical): the globally defined orbit is $z(\mu) = \mu$.

$r > 1$ (Escape): the globally defined orbit $z(\mu)$ has the limiting behavior $z(\mu) - |\mu| \to 0$ for $\mu \to \pm\infty$ and is stable backward in time. All orbits starting with $z < 0$ and $\mu \ll -1$ diverge to $+\infty$ in finite time after $\mu > -\sqrt{(r)}$.

In the original coordinates, the rescaled parameter $r = 1$ equals the first-order expansion for the critical rate $r_c(\epsilon)$,

$$r_c(\epsilon) = r_0 + \epsilon\sqrt{-\frac{r_0\Gamma''(\mu_{\rm crit})}{2a_0a_2}}.$$

If white noise of variance σ^2 is added to Eq. (A6),

$$dz = [a_0(r\Gamma(\mu) - r_0) + a_2z^2 + O(z^3)]dt + \sigma dW_t,$$

then σ^2 needs to be of the scale $\epsilon^{3/2}$. If $\sigma^2 = 2D[\epsilon c_n]^{3/2}$ with $c_n = (g_2r_0a_0)^{1/2}a_2^{-5/6}$ then the rescaled equation for z is

$$dz = [z^2 + r - \mu^2 + o(1)]dt + \sqrt{2D}dW_t.$$

1. Limitation of single-mode approximation

We use the saddle-node normal form Eqs. (A8) and (A9) to provide insight into the limitation of the single-mode approximation in reference to the maximal ramp speed r. The unique globally defined orbit $\tilde{z}(t)$ of Eqs. (A8) and (A9) for $\epsilon = 0$ is used to change to a comoving coordinate system,

$$y(t) = z(t) - \tilde{z}(t),$$

with respect to y such that Eqs. (A8) and (A9) have the form

$$\begin{aligned} \dot{z} &= z^2 + r - t^2, \\ \dot{\tilde{z}} + \dot{y} &= (\tilde{z} + y)^2 + r - t^2, \\ \dot{y} &= \tilde{z}^2 + 2\tilde{z}y + y^2 + r - t^2 - \dot{\tilde{z}}, \\ \dot{y} &= y^2 + 2\tilde{z}y = y(y + 2\tilde{z}). \end{aligned} \tag{A10}$$

The potential $U(y,t) = -\int y(y + 2\tilde{z})\,dy$ in the new coordinate system has a well at $y = 0$ and a hill top at $y = -2\tilde{z}$ for $\tilde{z} < 0$, but a hill top at $y = 0$ (and a well at $y = -2\tilde{z}$) for $\tilde{z} > 0$.

If white noise is added to Eq. (A10), the error of the single-mode approximation is small provided $|\dot{\tilde{z}}(t)|$ is small, which is the case for t close to the maximum of $\tilde{z}$. If $\tilde{z}(t) < 0$ for all t then escape is most likely to occur close to time $t_{\rm max}$, the maximum of $\tilde{z}(t)$ since the potential barrier is at its lowest. The mode approximation error at times close to $t_{\rm max}$ is small because $|\dot{\tilde{z}}(t)|$ is small, as discussed in the paper.

However, if $\tilde{z}(t) > 0$ for a range of t then escape occurs with a non-small probability at times when $|\dot{\tilde{z}}(t)|$ is not small. We identify that a maximal ramp speed $r \approx 0.59$ corresponds to $\max\{\tilde{z}(t) : t \in [t_0, T_{\rm end}]\} = 0$. Therefore, in the original coordinates the single-mode approximation fails for some maximal ramp speeds r less than r_c, and in particular, we consider only for parameters up to

$$r = r_0 + \tfrac{1}{2}\epsilon c_r,$$

where in the paper the constant r_1 is the same as c_r.

APPENDIX B: PHASE PLANES OF SHIFTED SYSTEM

In this section we consider all qualitatively different phase planes for the shifted slow-fast autonomous system

$$\dot{y} = f(y) + br\Gamma(\mu), \tag{B1}$$

$$\dot{\mu} = \epsilon\Gamma(\mu). \tag{B2}$$

Again we assume that in the limit $\epsilon = 0$, Eq. (B1) has a saddle-node bifurcation at $r\Gamma(\mu) = r_0 > 0$, $y = y_0$ with a stable branch $y^{(s)}[r\Gamma(\mu)]$ and an unstable branch $y^{(u)}[r\Gamma(\mu)]$ of equilibria emerging for $r\Gamma(\mu) \in [0,r_0]$. The properties Eq. (A3) of Γ imply that there exists three distinct sets of equilibria branches depending on the value of r in relation to r_0. These are presented in the (μ,y) phase plane in Fig. 9(a) for $r < r_0$, Fig. 9(b) for $r = r_0$, and Figs. 9(c)–9(e) for $r > r_0$. We will discuss the differences between Figs. 9(c)–9(e), but initially we will just focus on the branches of stable (blue dashed) and unstable (red dashed) equilibria for $\epsilon = 0$.

For $r < r_0$ in the limit $\epsilon = 0$ there exists one stable equilibrium and one unstable equilibrium for all $\mu \in [0,1]$; see Fig. 9(a). This means there is a continuous branch of stable equilibria connecting $(y,\mu) = (y^{(s)}[0],0)$ and $(y^{(s)}[0],1)$ and likewise an unstable branch connecting $(y,\mu) = (y^{(u)}[0],0)$ and $(y^{(u)}[0],1)$. The phase portrait in Fig. 9(a) corresponds to the case $r < 0$ for the rescaled r in the rescaled system Eqs. (A8) and (A9).

For $r = r_0$ the stable and unstable equilibria meet at $\mu_{\rm crit} \in (0,1)$ where $\Gamma(\mu_{\rm crit}) = 1$; see Fig. 9(b). In contrast to Fig. 9(a) the branches of equilibria approach at a linear rate and then also move away at a linear rate. This therefore means that the branches are nondifferentiable at $\mu = \mu_{\rm crit}$ but the continuous connections still exist.

In Figs. 9(c)–9(e), the maximal ramp speed r is greater than r_0 meaning that for μ in some interval $(\mu_l,\mu_u) \subset (0,1)$ centered around $\mu_{\rm crit}$ no equilibria exist in the limit $\epsilon = 0$. Instead two saddle-node bifurcations form at μ_l and μ_u with the branches of stable and unstable equilibria emerging for $\mu \in [0,\mu_l]$ and $\mu \in [\mu_u,1]$ to $y^{(s)}[0]$ and $y^{(u)}[0]$, respectively, at $\mu = 0$ and 1.

Let us now discuss the solid blue and red curves in Figs. 9(a)–9(e), which denote the unstable manifold of $(y,\mu) = (y^{(s)}[0],0)$ and the stable manifold of $(y,\mu) = (y^{(u)}[0],1)$ respectively. Figures 9(a)–9(c) depict the tracking scenario $(r < r_c)$ such that a connecting orbit exists between $y^{(s)}[0]$ at $\mu = 0$ and $y^{(s)}[0]$ at $\mu = 1$, the unstable manifold of

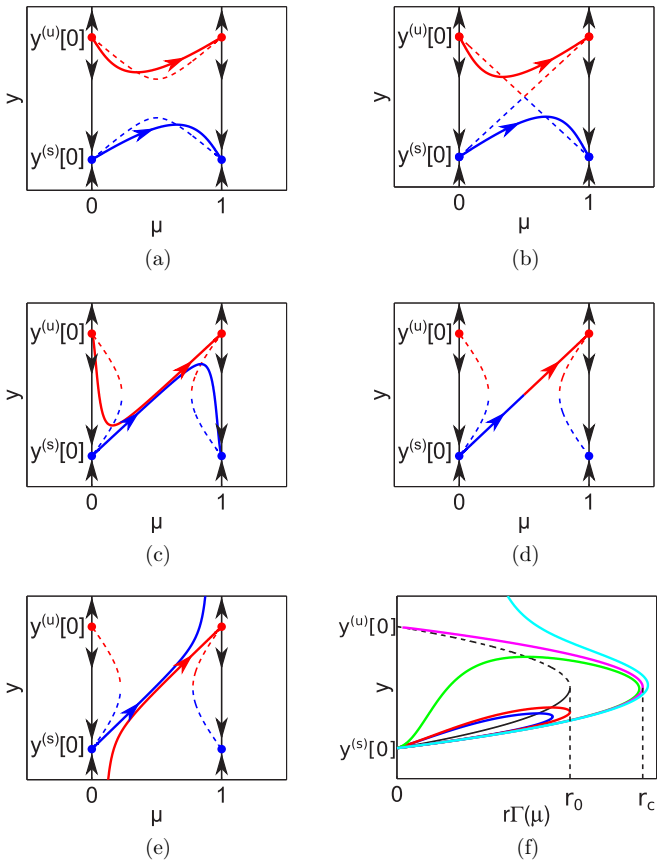

FIG. 9. (a)–(e) Qualitatively different phase planes of system Eqs. (B1) and (B2) dependent on the value of the maximal ramp speed r in relation to the saddle-node bifurcation at $r\Gamma(\mu) = r_0$ and the critical rate r_c that induces tipping [see panel (f)]. (a) $r < r_0 < r_c$, (b) $r = r_0 < r_c$, (c) $r_0 < r < r_c$, (d) $r_0 < r = r_c$, (e) $r_0 < r_c < r$. Blue (lower) and red (upper) dashed lines are the stable and unstable branches of equilibria in the limit $\epsilon = 0$. Solid blue and red curves represent the unstable manifold of the saddle $(y,\mu) = (y^{(s)}[0],0)$ and the stable manifold of the saddle $(y,\mu) = (y^{(u)}[0],1)$, respectively. Panel (f) provides the bifurcation diagram of Eqs. (B1) and (B2) in the $(r\Gamma(\mu),y)$ plane. Black solid curve denotes branch of stable equilibria and black dashed curve branch of unstable equilibria. Superimposed on top are trajectories of a realisation starting arbitrarily close to $(y,\mu) = (y^{(s)}[0],0)$ for panel (a) given in blue, (b) red, (c) green, (d) pink, (e) light blue (listed in increasing values of r). Parameter: $b = 1$.

$(y,\mu) = (y^{(s)}[0],0)$. The stable manifold of $(y,\mu) = (y^{(u)}[0],1)$ acts as a separatrix, where all solutions below the manifold converge to the stable node $(y,\mu) = (y^{(s)}[0],1)$ and all those above escape to infinity. For Figs. 9(a) and 9(b), solutions $(y(t),\mu(t))$ starting close to $(y^{(s)}[0],1)$ stay close to the stable equilibrium branch $y^{(s)}[r\Gamma(\mu(t))]$ for all t (distance goes to 0 as $\epsilon \to 0$). Notice in Fig. 9(c) that although $r > r_0$ such that the saddle-node bifurcation is crossed for a small period of time the system Eqs. (B1) and (B2) still does not tip because $r < r_c = r_0 + O(\epsilon)$ the critical rate. The scenario in Fig. 9(c) corresponds to the case $0 < r < 1$ for the rescaled r in the rescaled system Eqs. (A8) and (A9).

In Fig. 9(d) r equals r_c, which creates a saddle-to-saddle connection from $(y^{(s)}[0],0)$ to $(y^{(u)}[0],1)$. Finally, in Fig. 9(e) $r > r_c$, which induces system Eqs. (B1) and (B2) to tip. This means that initial conditions starting arbitrarily close to $(y^{(s)}[0],0)$ go on to escape following the unstable manifold of $(y^{(u)}[0],1)$. Figures 9(d) and 9(e) correspond to the critical case $r = 1$ (d) and the escape case $r > 1$ (e) for the rescaled r in the rescaled system Eqs. (A8) and (A9).

We present in Fig. 9(f) the bifurcation diagram of Eqs. (B1) and (B2) in the $(r\Gamma(\mu),y)$ plane. The black solid and dashed curves give the stable and unstable branches of equilibria, respectively. Superimposed on top are colored curves representing the trajectory for starting close to $(y,\mu) = (y^{(s)}[0],0)$ for each of the scenarios in Figs. 9(a)–9(e). The structure of the ramp means that solutions starting at $(r\Gamma(\mu),y) = (0,y^{(s)}[0])$ approach the saddle-node at $r\Gamma(\mu) = r_0$ at a slow speed initially, which gets faster until $\mu = \mu_{\text{crit}}$ is reached where $r\Gamma(\mu_{\text{crit}}) = r$ (the turning points of the colored curves; recall, μ_{crit} is where $\max\{\Gamma(\mu) : \mu \in [0,1]\} = 1$). The solutions then return back to $r\Gamma(1) = 0$.

A prominent feature in all cases is that initially the trajectory appears to lag behind the stable equilibrium branch $y^{(s)}[r\Gamma(\mu)]$ as $\Gamma(\mu(t))$ increases. The dark blue trajectory corresponds to Fig. 9(a) where $r < r_0$ and so in this scenario the saddle-node is not reached, which means the stable quasi-steady state is always present. Not evident from the bifurcation diagram is that when $\Gamma(\mu(t))$ reaches its maximum value the shift is at its fastest. Hence, the trajectory crosses the branch $y^{(s)}[r\Gamma(\mu(t))]$, since the quasisteady state changes direction quickly in comparison to the trajectory. The trajectory continues to lag until the ramp comes to a rest and the trajectory returns to $y^{(s)}[0]$ at $r\Gamma(1) = 0$. A similar pattern is observed for the red trajectory where $r = r_0$ [the scenario from Fig. 9(b)]. The lag becomes more pronounced the closer $r\Gamma(\mu(t))$ gets to r_0 the saddle node. Thus, only touching the saddle-node and not crossing it, combined with the speed of the shift, the trajectory will not escape and instead again cross the stable branch $y^{(s)}[r\Gamma(\mu(t))]$ and converge back to $y^{(s)}[0]$ at $r\Gamma(1) = 0$.

The green curve shows the trajectory for $r_0 < r < r_c$, which corresponds to Fig. 9(c). For $r\Gamma(\mu(t)) > r_0$ the trajectory gives the impression that it begins to escape but only slowly. Though once again this is deceptive since the speed of the ramp is at its fastest during this phase and so it is only a short period of time before $\Gamma(\mu(t)) = r_0$ for a second time. The quasisteady states then begin to emerge but the trajectory is now above the unstable quasisteady state. The trajectory continues to escape until it crosses the branch $y^{(u)}[r\Gamma(\mu(t))]$. This implies that the quasisteady state is shifting faster than the trajectory is escaping. Once across the unstable quasi-steady state the trajectory gets attracted back to $y^{(s)}[0]$ at $r\Gamma(1) = 0$ to complete the connecting orbit.

Whereas, the pink trajectory [$r = r_c$, Fig. 9(d)] is shifted a little bit further such that the trajectory meets the $y^{(u)}[r\Gamma(\mu(t))]$ branch only at the end of the ramp. The last scenario, $r > r_c$, the light blue trajectory is shifted sufficiently past the saddle-node bifurcation, such that the trajectory has enough time to escape before the system recovers.

[1] F. Kwasniok, Phys. Rev. E **88**, 052917 (2013).
[2] C. Folke, S. Carpenter, B. Walker, M. Scheffer, T. Elmqvist, L. Gunderson, and C. Holling, Ann. Rev. Ecol. Evol. Systemat. **35**, 557 (2004).
[3] M. Hirota, M. Holmgren, E. H. Van Nes, and M. Scheffer, Science **334**, 232 (2011).
[4] R. M. May, S. A. Levin, and G. Sugihara, Nature **451**, 893 (2008).
[5] P. Ashwin, S. Wieczorek, R. Vitolo, and P. Cox, Philos. Trans. R. Soc. London A **370**, 1166 (2012); correction coauthored with C. Perryman (Née Hobbs) *ibid.* **371**, 20130098 (2013).
[6] T. M. Lenton, Ann. Rev. Environ. Res. **38**, 1 (2013).
[7] P. Ashwin, C. Perryman, and S. Wieczorek, Nonlinearity **30**, 2185 (2017).
[8] M. Scheffer, J. Bascompte, W. A. Brock, V. Brovkin, S. R. Carpenter, V. Dakos, H. Held, E. H. Van Nes, M. Rietkerk, and G. Sugihara, Nature **461**, 53 (2009).
[9] I. A. van de Leemput, M. Wichers, A. O. Cramer, D. Borsboom, F. Tuerlinckx, P. Kuppens, E. H. van Nes, W. Viechtbauer, E. J. Giltay, S. H. Aggen *et al.*, Proc. Natl. Acad. Sci. USA **111**, 87 (2014).
[10] P. Ritchie and J. Sieber, Chaos **26**, 093116 (2016).
[11] M. Scheffer, S. R. Carpenter, T. M. Lenton, J. Bascompte, W. Brock, V. Dakos, J. Van De Koppel, I. A. Van De Leemput, S. A. Levin, E. H. Van Nes *et al.*, Science **338**, 344 (2012).
[12] T. Lenton, V. Livina, V. Dakos, E. Van Nes, and M. Scheffer, Philos. Trans. R. Soc. London A **370**, 1185 (2012).
[13] V. Dakos, S. R. Carpenter, E. H. van Nes, and M. Scheffer, Philos. Trans. R. Soc. London B **370**, 20130263 (2015).
[14] Y. Sharma, P. S. Dutta, and A. K. Gupta, Phys. Rev. E **93**, 032404 (2016).
[15] C. Perryman and S. Wieczorek, Proc. R. Soc. London, Ser. A **470**, 20140226 (2014).
[16] V. Dakos, M. Scheffer, E. H. van Nes, V. Brovkin, V. Petoukhov, and H. Held, Proc. Natl. Acad. Sci. USA **105**, 14308 (2008).
[17] P. D. Ditlevsen and S. J. Johnsen, Geophys. Res. Lett. **37**, L19703 (2010).
[18] C. Boettiger and A. Hastings, Proc. R. Soc. London, Ser. B **279**, 4734 (2012).
[19] C. Boettiger and A. Hastings, Proc. R. Soc. London, Ser. B **280**, 20131372 (2013).
[20] J. M. Drake, Proc. R. Soc. London, Ser. B **280**, 20130686 (2013).
[21] S. Wieczorek, P. Ashwin, C. M. Luke, and P. M. Cox, in *Proceedings of the Royal Society of London A: Mathematical, Physical and Engineering Sciences* (The Royal Society, London, 2011), Vol. 467, pp. 1243–1269.
[22] H. Risken and T. Frank, *The Fokker-Planck Equation: Methods of Solution and Applications* (Springer Science & Business Media, Berlin, 2012).
[23] D. Zhang, G. Wei, D. Kouri, and D. Hoffman, J. Chem. Phys. **106**, 5216 (1997).
[24] G. Williams, *Linear Algebra with Applications* (Jones & Bartlett Publishers, Burlington, MA, 2012).
[25] C. G. Perryman, Ph.D. thesis, University of Exeter, 2015.